M-shell ionization of heavy elements by 0.1–1.0 MeV/amu ^{1,2}H and ^{3,4}He ions

M. Pajek,* D. Banaś, J. Braziewicz, and M. Czarnota
Institute of Physics, Świętokrzyska Academy, 25-406 Kielce, Poland

A. Bieńkowski, M. Jaskóła, and A. Korman
The Andrzej Soltan Institute for Nuclear Studies, 05-400 Otwock-Świerk, Poland

D. Trautmann
Institut für Theoretische Physik, Universität Basel, CH-4056 Basel, Switzerland

G. Lapicki
Department of Physics, East Carolina University, Greenville, North Carolina 27858, USA
(Received 3 October 2005; published 17 January 2006)

The *M*-shell ionization in high-*Z* atoms by low-energy light $^{1}_{1}$H, $^{2}_{1}$H, $^{3}_{2}$He, and $^{4}_{2}$He ions have been studied *systematically* in the energy range 0.1–1.0 MeV/amu in order to verify the available theoretical approaches describing the *M*-shell ionization by charged particles in asymmetric collisions. The present low-energy data, combined with our earlier results reported for *M*-shell ionization by hydrogen and helium ions for higher energies, form a systematic experimental basis to test the theoretical predictions of *M*-shell ionization based on the plane-wave Born approximation (PWBA), the semiclassical approximation (SCA), and the binary-encounter approximation (BEA). In the PWBA based approaches the energy loss (E), Coulomb deflection (C), perturbed stationary state (PSS), and relativistic (R) effects were considered within the ECPSSR theory and its recent modification, called the ECUSAR theory, in which a description of the PSS effect was corrected to account for the united- and separated-atom (USA) electron binding energy limits. In the SCA calculations with relativistic wave functions the binding effect was included only in the limiting cases of separated-atom and united-atom limits. Possible contribution of the electron capture, multiple ionization, and recoil ionization to the *M*-shell vacancy production, which is dominated for light ions impact by direct single ionization process, are also discussed. The universal scaling of measured *M*-shell x-ray production and ionization cross sections was investigated in detail. Using the present data the *isotopic effect* has been studied by comparing the measured *M*-shell ionization cross-section ratios for equal-velocity hydrogen $^{1}_{1}$H and $^{2}_{1}$H as well as helium $^{3}_{2}$He and $^{4}_{2}$He isotopes. In addition, the ratios of measured ionization cross sections for $^{2}_{1}$H and $^{4}_{2}$He were used to investigate the role of the *binding effect*. The present results are of practical importance for the application of particle-induced x-ray emission technique in trace element studies.

DOI: 10.1103/PhysRevA.73.012709 PACS number(s): 34.50.Fa

I. INTRODUCTION

The excitation of x rays by charged particles is of great theoretical and practical interest. For light-ion impact this fundamental process of interaction of charged particles with atoms is dominated by direct Coulomb ionization leading to creation of single-vacancy configuration, which decays radiatively via emission of x rays or nonradiatively by the Auger or Coster-Kronig processes. The inner-shell ionization and x-ray production by charged particles has been extensively studied in the last three decades, mainly because of its importance for the particle induced x-ray emission (PIXE) in analytical studies. Earlier theoretical and experimental results concerning the inner-shell ionization by ion impact as well as the x-ray emission can be found in Refs. [1,2]. A knowledge of the cross sections for ionization induced by light as well heavy ions offers an experimental basis for developing and testing the theoretical descriptions of both ionization and inner-shell de-excitation processes. Most of earlier experiments were performed for light ion impact for *K* and *L* shells (see the available compilations [3–9]. With increased availability of heavy-ion beams, the inner-shell ionization measurements have been extended to heavier ions [10,11], for which the process of excitation of x rays becomes more complex due to the increasing role of the multiple ionization and the electron capture processes.

Early experiments concerning the *M*-shell ionization were performed for light-ion impact, mainly protons and alpha particles, using thick targets and scintillation counters [12] and gas proportional detectors [13–16]. With the advent of semiconductor Si(Li) detectors more accurate and reliable data became available for *M*-shell ionization both for light [17–28] and heavy ions [29–34]. In these experiments the thin targets were typically used improving substantially a quality of the data. Nevertheless, the *M*-shell x-ray production or ionization cross sections available in the literature are substantially scattered, exceeding sometimes a level of quoted experimental uncertainties. This can be related, in our opinion, with possible deficiencies in determination of x-ray detector efficiency for low-energy *M*-x rays, being typically

*Electronic address: pajek@pu.kielce.pl

within the range of 1–3 keV. Following the developed method of accurate determination of the efficiency of a Si(Li) detector (see Ref. [35]) for low-energy x rays, i.e., the region important for M x rays, in the last years we have studied the M-shell ionization by light ions in the energy range 0.6–4.0 MeV [36–41]. From that time more experimental results [42–51] reported by other authors appeared. The main motivation of the present study was the accurate and systematic measurements of the M-shell x-ray production and ionization cross sections for low-energy hydrogen and helium ions to obtain the systematic data at the equal-velocity conditions for $^{1}_{1}$H, $^{2}_{1}$H, $^{3}_{2}$He, and $^{4}_{2}$He ions in the energy range 0.1–1.0 MeV/amu. The precise and systematic experimental M-shell ionization cross sections for light ions are very important for testing theoretical predictions. These results from the fact that for such strongly asymmetric collisions both the multiple ionization and electron capture play a negligible role and thus the dynamics of the direct ionization process can be studied.

The theoretical approaches developed to describe the inner-shell ionization by heavy, charged projectiles have been focused on the description of asymmetric collisions ($Z_1 \ll Z_2$), where Z_1 and Z_2 are the projectile and target atomic numbers, respectively. In such collisions the inner-shell vacancies are produced predominantly by the direct Coulomb ionization process, which can be treated perturbatively using the first-order perturbation approaches, namely the plane-wave Born approximation (PWBA) [52] and the semiclassical approximation (SCA) [53]. Besides the quantum-mechanical treatment the classical nonperturbative approach, known as the binary-encounter approximation (BEA) [54,55] was developed for describing direct ionization. This model treats the ionization process in a more simplified way and will not be discussed here. The standard PWBA [56–58] and SCA [59–62] approaches for direct ionization were further developed to include the hyperbolic trajectory of the projectile [63–65], the relativistic wave functions [64,66–69] and the corrections for the "binding-polarization effect" [70–72]. The most advanced approach based on the PWBA, which goes beyond the first-order treatment to include the corrections for the binding-polarization effects, within the perturbed stationary states (PSS) approximation, the projectile energy loss (E) and Coulomb deflection (C) effects, as well as the relativistic (R) description of inner-shell electrons is known as the ECPSSR theory [73]. This theory has been recently modified within the ECUSAR theory [74] which includes the effect of saturation of the electron binding energy at the united atom value. On the other hand, the state-of-the-art SCA calculations which are presently available (see Refs. [75–78]) use the hyperbolic projectile trajectory and relativistic electronic wave functions in an exact way, but the binding effect can be treated within the extreme cases of separated atom (SA) or united atom (UA) limits.

The ionization of the K and L shells by light ions is rather well described theoretically in a broad range of projectile energies and target atomic numbers. Heavier projectiles, however, perturb initial electronic states more strongly and consequently the ECPSSR and SCA theories cannot describe these data as well as for lighter ions. This was particularly well evidenced for L-subshell ionization by low-velocity heavy ions [79]. The discrepancies observed for L-subshell ionization relate to the fact that the theoretical approaches mentioned above treat the ionization of L subshells independently neglecting the intrashell coupling effects. Since wave functions of the L subshells are very close to each other both in energy and space the dynamical couplings between the states strongly modify the initial L-shell vacancy distribution. In fact, such an effect of the L-subshell couplings was treated theoretically using various approaches, from a simple two-step model of Sarkadi and Mukoyama [79] to full coupled-channel calculations of Martir *et al.* [80] and Mehler *et al.* [81]. A simplified coupled-channels calculation, known as the "coupled-subshells model" (CSM), which was proposed by Sarkadi and Mukoyama [82–85], has been recently discussed by Pajek *et al.* [86] in the context of L-shell ionization of heavy atoms by oxygen ions. In general, the subshell couplings do not influence the total ionization cross sections for a given shell and consequently this effect is not expected to play a role for the total M-shell ionization cross sections discussed in the present work.

The present paper summarizes our earlier and present results concerning the systematic measurements of the M-shell ionization in heavy atoms ($_{73}$Ta, $_{74}$W, $_{75}$Re, $_{76}$Os, $_{77}$Ir, $_{78}$Pt, $_{79}$Au, $_{83}$Bi, and $_{90}$Th) by light $^{1}_{1}$H, $^{2}_{1}$H, $^{3}_{2}$He, and $^{4}_{2}$He ions in the energy range 0.1–1.0 MeV/amu. More precisely, the measurements of the M-shell ionization cross sections for low-energy hydrogen and helium ions are reported here, which combined with the results of our earlier experiments [36–38], form a set of systematic data for the same energy-to-mass ratios for different $^{1}_{1}$H, $^{2}_{1}$H, $^{3}_{2}$He, and $^{4}_{2}$He projectiles. The measured M x-ray production and M-shell ionization cross sections allow one to perform a critical discussion of the available theoretical approaches describing the M-shell ionization by charged particles. On the other hand, these results are of practical interest for calculation of the accurate empirical M x-ray production cross sections for PIXE applications.

The paper is organized as follows. The experimental aspects of this work are described in Sec. II, while the data analysis and the results are discussed in Sec. III. In the following Sec. IV the available theoretical approaches (PWBA, SCA, BEA, ECPSSR) treating the M-shell ionization are discussed. Next, a discussion of the M-shell fluorescence, (super-) Coster-Kronig and x-ray emission rates, used to derive the M-shell ionization cross sections for the M shell, are summarized in Sec. V. This section gives a systematic comparison of the measured data with theoretical predictions in a form of the universal M-shell ionization cross sections as well as a discussion of the isotopic and binding effects. Finally, the paper is summarized in Sec. VI.

II. EXPERIMENT

The beams of single ionized $^{1}_{1}$H, $^{2}_{1}$H, $^{3}_{2}$He, and $^{4}_{2}$He light ions obtained from the 3-MeV Van de Graaff accelerator at the Andrzej Soltan Institute of Nuclear Studies (SINS) in Warsaw were used to excite the M x rays in heavy atoms studied. The ion-beam energies, selected in such a way to

cover together with our earlier measurements [36–38] the energy range 0.1–1.0 MeV/amu, were the following: 0.1–0.6 MeV for $^{1}_{1}$H, 0.2–2.0 MeV for $^{2}_{1}$H, 0.3–0.6 MeV for $^{3}_{2}$He, and 0.4–0.8 MeV for $^{4}_{2}$He (see Tables I and II). The energy steps were selected as 25–100 keV/amu to cover systematically the energy range from 0.1 to 1.0 MeV/amu.

In order to extend the ion-beam energies below 0.4 MeV the following modifications of the accelerator were performed concerning both ion beam stability and its energy definition: (i) an extra aluminum electrode of about 20 cm diameter was installed at the high voltage electrode opposite the corona triode, (ii) to increase the ion-beam current for energies below 0.3 MeV a shorting wire assembly inside the high-pressure vessel has been installed, (iii) a Hall probe was used, instead of a NMR magnetometer, for the magnetic-field strength measurements below 0.1 T. With these modifications it was possible to obtain stable low-energy ion beam collimated to a 2-mm diameter with intensities 20–200 nA on the target. The 90° analyzing magnet of the accelerator, having a bending radius r=50 cm, was calibrated using the ^{27}Al$(p,\gamma)^{28}$Si and ^{19}F$(p,\alpha\gamma)^{16}$O nuclear reactions with recommended resonance energies E_r=991.90±0.04 keV and 340.46±0.04 keV, respectively, taken from Marion [87]. The ion beam excited the M x rays in a thin layer (3–30 μg/cm^2) of target material ($_{73}$Ta, $_{74}$W, $_{75}$Re, $_{76}$Os, $_{77}$Ir, $_{78}$Pt, $_{79}$Au, $_{83}$Bi, and $_{90}$Th) evaporated onto 20–30 μg/cm^2 carbon backing. The targets were mounted at an angle 30° with respect of beam direction.

The M x rays excited in the targets were detected by a 30-cm^2 Tracor Si(Li) x-ray detector, having a 25-μm beryllium window and an energy resolution of 180 eV for 5.9 keV. The detector was mounted outside the vacuum chamber, perpendicularly to the ion-beam direction. In measurements of the M x rays induced by deuterons an optimized beam transport system (good focusing) and a high vacuum (below 10^{-5} Torr) in both the tube and the target chamber were found to be very important for suppressing the deuteron beam scattering, and thus reducing the nuclear reactions background in the shielded Si(Li) detector. However, at relatively high incident deuteron energies, the increased background in the photon spectrum is an unavoidable effect mainly due to increased production of neutrons by the scattered deuteron beam in the beam tube. To suppress these neutrons special shielding consisting of layers of concrete, polyethylene, and cadmium, 25, 6, and 0.1 cm thick, respectively, were mounted in the most critical areas of the tube. The Faraday cup and Si(Li) detector were also covered with a 6-cm-thick polyethylene layer and 1-mm-thick cadmium plating.

A number of ions impinging on the target was monitored by a surface barrier Si detector detecting the projectiles backscattered at an angle 150° with respect to the ion-beam axis. A typical spectra of M x rays, L x rays, as well as elastically backscattered projectiles are shown in Fig. 1 for 1-MeV protons impact and gold target.

The efficiency of a Si(Li) x-ray detector was measured by means of two complimentary methods covering the photon energy range 1–60 keV, following the procedure described in Ref. [35]. We emphasize here a fact that the measurements of Si(Li) detector efficiency in a wide energy range is very crucial for accurate (5%) modeling [35] of the low-energy part (1–5 keV) of detector efficiency corresponding to the M x rays studied. First, the calibrated (±1.8%) x-ray sources of ^{133}Ba, ^{152}Eu, and ^{241}Am were used to determine the efficiency for x-ray energies above 12 keV. The x-ray detector efficiency in the photon energy range between 1.5 and 17 keV was measured by bombarding thin targets of low-Z and mid-Z elements with 2-MeV $^{4}_{2}$He ions. From the measured K x-ray yields, normalized to a number of elastically backscattered ions, the efficiency of a Si(Li) detector was determined using the "reference" K-shell ionization cross sections (see Ref. [88]) and the screened elastic cross sections [89]. By using this method we were able to determine the efficiency of a Si(Li) detector in the energy range 1–5 keV with total uncertainties 5–3 %. The measured and fitted efficiency of a Si(Li) detector used in the present study is shown in Fig. 2.

III. DATA ANALYSIS AND RESULTS

The M x rays excited in heavy atoms (Ta-Th) form a complex structure which cannot be well resolved by a semiconductor x-ray detector (see Fig. 1). In order to interpret the measured M x-ray spectra a diagram of M x-ray transitions in heavy atoms is shown in Fig. 3 together with estimated relative intensities of individual x-ray lines. In general, a spectrum of M x rays is dominated by strong $M_{\alpha,\beta}(M_{4,5}N_{6,7})$ x-ray transitions and less intense, but clearly visible, M x-ray lines indicated as $M_{\zeta_{2,1}}(M_{4,5}N_{2,3})$, M_3N_1, $M_\gamma(M_3N_{4,5})$, $M_3O_{4,5}+M_2N_4$, M_2O_4, and $M_1O_{2,3}$ x-ray transitions. Consequently, these M x-ray transitions were fitted to the measured spectra by assuming a Gaussian line shape and polynomial background. As an example, the results of such analysis of measured M x-ray spectrum excited by 1-MeV/amu $^{2}_{1}$H ions on gold is shown in Fig. 4. In this way the x-ray intensities for individual M x-ray lines were obtained which were further used to determine the total M-ray production cross sections.

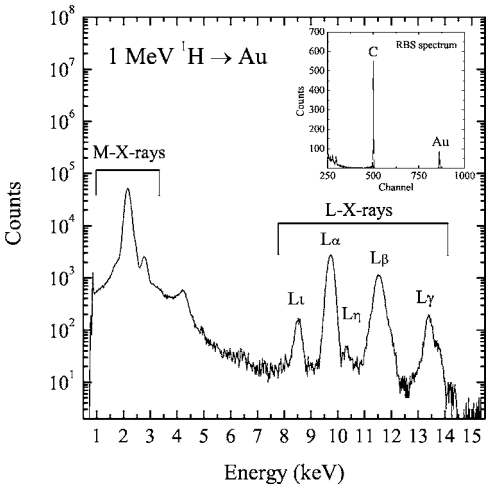

FIG. 1. The x-ray spectrum of M and L x-rays of gold excited by 1-MeV protons measured by a Si(Li) detector. The inset shows the energy spectrum of elastically backscattered projectiles used to normalize the measured x-ray yields.

TABLE I. The total M-shell x-ray production cross sections σ_{MX} (in barns) measured for $_{73}$Ta, $_{74}$W, $_{75}$Re, $_{76}$Os, $_{77}$Ir, $_{78}$Pt, $_{79}$Au, $_{83}$Bi, and $_{90}$Th atoms bombarded by $^{1}_{1}$H and $^{2}_{1}$H ions in the energy range 0.1–1.0 MeV/amu. The cross sections for protons for the energies higher than 0.700 MeV/amu are taken from our earlier work [36]. The ranges of experimental uncertainties are shown in the table. Note: 2.88+1 denotes 2.88×10^{1} barns.

				$^{1}_{1}$H ions					
Energy (MeV/amu)	$_{73}$Ta	$_{74}$W	$_{75}$Re	$_{76}$Os	$_{77}$Ir	$_{78}$Pt	$_{79}$Au	$_{83}$Bi	$_{90}$Th
0.100	1.29+1	1.06+1		8.60+0	6.72+0	6.03+0	5.44+0	1.82+0	1.53−1
0.125	2.48+1	2.24+1		1.96+1	1.71+1	1.48+1	1.29+1	6.00+0	1.07+0
0.150	3.67+1	3.36+1		2.89+1	2.65+1	2.29+1	2.00+1	1.10+1	2.53+0
0.175	4.75+1	4.57+1		3.98+1	3.63+1	3.16+1	2.89+1	2.02+1	5.08+0
0.200	6.37+1	5.56+1		5.06+1	4.48+1	4.11+1	3.86+1	2.91+1	7.09+0
0.225	8.44+1	7.63+1		6.76+1	6.15+1	5.74+1		3.88+1	1.08+1
0.250	1.16+2	1.13+2		1.05+2	9.70+1	8.53+1	7.96+1	6.75+1	1.80+1
0.300	1.65+2	1.53+2		1.46+2	1.35+2	1.22+2	1.19+2	7.58+1	3.01+1
0.350	2.25+2	2.17+2		2.10+2	1.90+2	1.74+2		1.08+2	4.88+1
0.400	2.75+2	2.70+2		2.53+2	2.39+2	2.27+2	2.22+2	1.46+2	6.73+1
0.450	3.26+2	2.90+2		3.15+2	2.74+2	2.62+2	2.53+2	1.75+2	8.73+1
0.500	3.83+2	3.50+2		3.33+2	3.04+2	2.83+2	2.89+2	1.95+2	1.06+2
0.600	4.70+2	4.52+2		4.28+2	3.87+2	3.85+2	3.57+2	2.57+2	
0.600	4.34+2	4.39+2	4.86+2	4.52+2	4.10+2	3.94+2	3.82+2	2.82+2	1.52+2
0.700	5.33+2	5.39+2	5.83+2	5.63+2	5.12+2	4.90+2	4.85+2	3.51+2	1.98+2
0.800	6.31+2	6.16+2	6.77+2	6.16+2	6.01+2	5.53+2	5.42+2	4.00+2	2.44+2
0.900	7.34+2	7.18+2	7.58+2	7.14+2	7.02+2	6.47+2	6.29+2	4.72+2	2.84+2
1.000	8.27+2	7.95+2	8.68+2	8.23+2	7.55+2	7.00+2	6.73+2	5.46+2	3.47+2
Uncertainty (%)	9–12	10–13	10–25	7–9	10–12	10–12	10–15	8–10	8–10
				$^{2}_{1}$H ions					
Energy (MeV/amu)	$_{73}$Ta	$_{74}$W	$_{75}$Re	$_{76}$Os	$_{77}$Ir	$_{78}$Pt	$_{79}$Au	$_{83}$Bi	$_{90}$Th
0.100	1.92+1			1.50+1			9.31+0	4.97+0	7.50−1
0.125	3.53+1	2.91+1	3.27+1	2.95+1	2.52+1		1.94+1	1.14+1	2.35+0
0.150		4.64+1		4.90+1	4.22+1		3.11+1	1.76+1	5.19+0
0.175	7.49+1	6.20+1	7.14+1	6.67+1	5.59+1		4.34+1	2.95+1	8.30+0
0.200	9.44+1	7.90+1	8.74+1	8.45+1	6.15+1		5.88+1	3.66+1	1.32+1
0.225	1.17+2	9.65+1	1.11+2	1.08+2	9.17+1		7.72+1	4.97+1	1.89+1
0.250	1.47+2	1.21+2	1.38+2	1.31+2	1.20+2		9.72+1	6.57+1	2.51+1
0.300	2.04+2	1.68+2	1.97+2	1.91+2	1.70+2		1.42+2	9.78+1	4.02+1
0.350	2.63+2	2.19+2	2.65+2	2.46+2	2.13+2		1.88+2	1.29+2	6.40+1
0.400	3.09+2	2.64+2	3.09+2	2.91+2	2.72+2		2.34+2	1.68+2	8.61+1
0.450	3.62+2	3.21+2	3.91+2	3.23+2	3.37+2		2.73+2	1.94+2	1.05+2
0.500	4.14+2	3.53+2	4.18+2	3.89+2	3.77+2		3.03+2	2.20+2	1.41+2
0.600	5.37+2	4.88+2	5.42+2	5.13+2	4.81+2		4.07+2	3.01+2	1.67+2
0.700	6.64+2	6.09+2	6.96+2	6.09+2	5.92+2		4.80+2	3.58+2	2.48+2
0.800	7.60+2	6.88+2	7.73+2	6.72+2	7.11+2		5.96+2	4.09+2	2.87+2
0.900	8.06+2	7.48+2	8.41+2	7.96+2	8.54+2		6.67+2	4.97+2	3.52+2
1.000	9.80+2	9.49+2	1.05+3	9.50+2	9.58+2		8.02+2	5.51+2	3.71+2
Uncertainty (%)	10–12	10–12	10–15	7–9	10–12		11–25	7–10	7–10

It should be noticed that a possible nonisotropic emission of individual M x-ray lines has to be taken into account in calculating the total M-ray production cross sections. In general, due to the effect of collisional alignment resulting in anisotropy of emitted x rays for initial vacancy with total angular momentum $j>1/2$ [90,91], the x rays emitted from M_3, M_4, and M_5 subshell are anisotropic. However, as it was demonstrated by Wigger *et al.* [92] and Blümke *et al.* [93] the anisotropy of M x rays for 0.15–1.0-MeV proton impact on Th and Au, respectively, is rather small with the absolute

TABLE II. The total *M*-shell x-ray production cross sections σ_{MX} (in barns) measured for $_{73}$Ta, $_{74}$W, $_{75}$Re, $_{76}$Os, $_{77}$Ir, $_{78}$Pt, $_{79}$Au, $_{83}$Bi, and $_{90}$Th atoms bombarded by $^{3}_{2}$He and $^{4}_{2}$He ions in the energy range 0.1–1.0 MeV/amu. The cross sections for the energies higher than 0.225 MeV/amu are taken from our earlier works [37,38]. The ranges of experimental uncertainties are shown in the table. Note: 2.88+1 denotes 2.88×10^{1} barns.

					$^{3}_{2}$He ions				
Energy (MeV/amu)	$_{73}$Ta	$_{74}$W	$_{75}$Re	$_{76}$Os	$_{77}$Ir	$_{78}$Pt	$_{79}$Au	$_{83}$Bi	$_{90}$Th
0.100	5.29+1	5.15+1	4.16+1	4.18+1			2.35+1	1.14+1	1.45+0
0.125	9.62+1	9.54+1	6.72+1	8.05+1			5.36+1	2.98+1	4.85+0
0.150	1.44+2	1.44+2	1.30+2	1.31+2			9.12+1	5.39+1	1.25+1
0.175	2.23+2	2.11+2	1.87+2	1.96+2			1.46+2	8.12+1	2.53+1
0.200	2.92+2	2.84+2	2.62+2	2.63+2			2.00+2	1.17+2	3.97+1
0.200	2.59+2			2.68+2			1.96+2	1.20+2	4.10+1
0.225	3.82+2	3.49+2	3.34+2	3.37+2			2.59+2	1.56+2	5.92+1
0.250	4.10+2			4.07+2			3.07+2	2.06+2	8.13+1
0.300	5.60+2			5.62+2			4.38+2	2.95+2	1.29+2
0.350	7.64+2			7.67+2			6.03+2	4.11+2	1.93+2
0.400	1.02+3			9.60+2			7.58+2	5.12+2	2.57+2
0.450	1.17+3			1.15+3			9.25+2	6.17+2	3.22+2
0.500	1.37+3			1.38+3			1.12+3	7.03+2	4.08+2
0.600	1.98+3			1.81+3			1.49+3	1.02+3	5.51+2
0.700	2.29+3			2.22+3			1.89+3	1.28+3	7.40+2
0.800	2.81+3			2.79+3			2.40+3	1.66+3	9.48+2
0.900	3.26+3			3.25+3			2.86+3	1.94+3	1.12+3
1.000	3.80+3			3.84+3			3.32+3	2.26+3	1.31+3
Uncertainty(%)	9–12	10–13	10–25	7–9			10–15	8–10	8–10
					$^{4}_{2}$He ions				
Energy (MeV/amu)	$_{73}$Ta	$_{74}$W	$_{75}$Re	$_{76}$Os	$_{77}$Ir	$_{78}$Pt	$_{79}$Au	$_{83}$Bi	$_{90}$Th
0.100	5.38+1	5.41+1		4.69+1	3.78+1	3.25+1	2.83+1	1.41+1	2.09+0
0.125	1.10+2	1.02+2		9.25+1	7.30+1	6.68+1	6.24+1	3.06+1	7.03+0
0.150	1.54+2	1.56+2		1.28+2	1.14+2	1.14+2	9.91+1	5.35+1	1.49+1
0.175	2.20+2	2.00+2		1.88+2	1.71+2	1.47+2	1.49+2	8.22+1	2.55+1
0.200	2.95+2	2.75+2		2.61+2	2.33+2	2.12+2	1.95+2	1.17+2	3.94+1
0.200	2.84+2			2.59+2	2.51+2	2.22+2	2.10+2	1.20+2	4.57+1
0.225	3.80+2	3.57+2		3.33+2	3.14+2	2.68+2	2.59+2	1.59+2	5.98+1
0.250	4.47+2			4.15+2	4.06+2	3.55+2	3.35+2	2.20+2	9.09+1
0.300	6.24+2			5.93+2	5.55+2	5.03+2	4.73+2	3.03+2	1.42+2
0.350	8.35+2			7.91+2	7.45+2	6.52+2	6.14+2	4.42+2	2.09+2
0.400	1.04+3			9.93+2	9.16+2	8.41+2	7.96+2	5.57+2	2.80+2
0.450	1.23+3			1.16+3	1.09+3	9.90+2	9.46+2	6.95+2	3.54+2
0.500	1.41+3			1.38+3	1.30+3	1.20+3	1.12+3	7.75+2	4.34+2
0.550	1.61+3			1.56+3	1.43+3	1.31+3	1.26+3	9.26+2	5.18+2
0.600	1.82+3			1.77+3	1.75+3	1.63+3	1.57+3	1.05+3	6.07+2
0.650	2.06+3			1.98+3	1.94+3	1.77+3	1.71+3	1.21+3	7.00+2
0.700	2.28+3			2.22+3	2.18+3	1.99+3	1.93+3	1.35+3	7.97+2
0.750				2.52+3	2.31+3	2.21+3	2.11+3	1.50+3	8.80+2
0.800	2.91+3			2.77+3	2.65+3	2.50+3	2.36+3	1.66+3	9.81+2
0.850	3.14+3			3.02+3	2.75+3	2.53+3	2.35+3	1.74+3	1.07+3
0.900	3.32+3			3.24+3	2.97+3	2.74+3	2.63+3	1.94+3	1.18+3
0.950	3.58+3			3.37+3	3.24+3	3.10+3	2.95+3	2.11+3	1.26+3
1.000	3.77+3			3.52+3	3.53+3	3.27+3	3.19+3	2.24+3	1.39+3
Uncertainty (%)	10–12	10–12		7–9	10–12	10–12	11–25	7–10	7–10

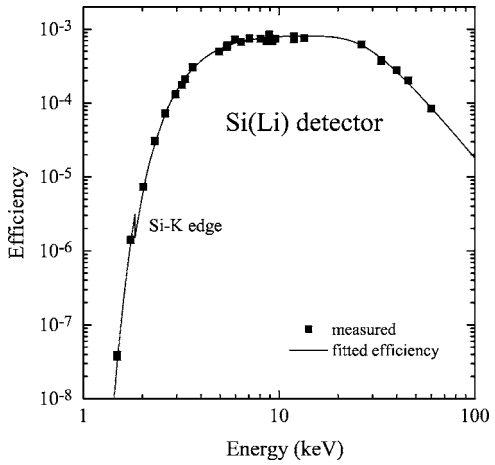

FIG. 2. The measured and fitted efficiency of a Si(Li) detector used in the present study. The fitted curve was obtained using a model of Si(Li) detector efficiency described in Ref. [35].

value of the alignment parameter $\mathcal{A}_{20}$ [91] being less than 0.4 [92]. Using these results we have estimated that the alignment effect could introduce a correction to the measured total M-shell x-ray production cross sections being less than 3%, and consequently it was neglected in further data analysis.

The measured cross sections were corrected for the effects of projectile energy loss and x-ray self-absorption in a finite target thickness following the procedure described in Ref. [36]. This correction was very small, being in the range of 1–3 %. Finally, the summed total M x-ray production cross sections were obtained with overall experimental uncertainties 7–15 %, which were mostly dominated by the uncertainties associated with determination of a Si(Li) detector efficiency.

In order to illustrate the typical results, the x-ray production cross sections measured for dominating M x-ray lines, namely $M_{\alpha,\beta}(M_{4,5}N_{6,7})$, $M_{\gamma}(M_3N_{4,5})$, $M_3O_{4,5}+M_2N_4$, M_2O_4, and $M_1O_{2,3}$ for protons on Au in the energy range

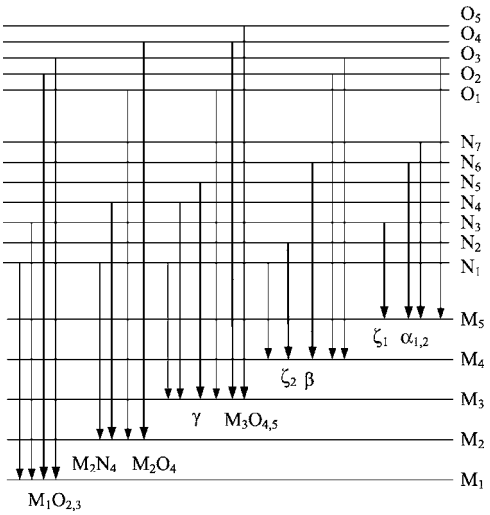

FIG. 3. A scheme of energy levels in M, N, and O shells showing the diagram M x-ray transitions.

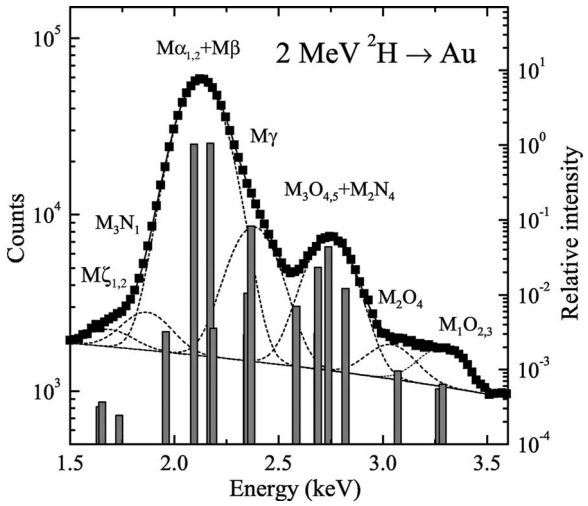

FIG. 4. Measured spectrum of M x rays of gold bombarded by 1-MeV/amu deuterons with resolved, dominating x-ray lines, namely $M_{\alpha,\beta}(M_{4,5}N_{6,7})$, $M_{\gamma}(M_3N_{4,5})$, $M_3O_{4,5}+M_2N_4$, M_2O_4, $M_1O_{2,3}$, $M_{\zeta_{2,1}}(M_{4,5}N_{2,3})$, and M_3N_1. The complete structure of the M-shell diagram lines, with theoretical relative intensities taken from PWBA [58], is also shown in the figure for a comparison.

0.1–1.0 MeV/amu, are shown in Fig. 5. This figure also shows the theoretical predictions according to the basic PWBA, SCA, and ECPSSR approaches, which will be discussed in detail in Sec. IV. Additionally, in Fig. 6, the measured total M x-ray production cross sections for gold bombarded by protons are compared with the results reported in literature by other authors [19,21–24,27,36,44,46,51] in a wider energy range, 0.1–40 MeV. This figure clearly demonstrates a substantial disagreement existing between the data reported by different authors thus justifying a need for more precise and reliable measurements of M x-ray production cross sections. The numerical values of measured total M x-ray production cross sections σ_{MX} for $_{73}$Ta, $_{74}$W, $_{75}$Re, $_{76}$Os, $_{77}$Ir, $_{78}$Pt, $_{79}$Au, $_{83}$Bi, and $_{90}$Th bombarded by 0.1–1.0-MeV $_1^1$H, $_1^2$H, $_2^3$He, and $_2^4$He ions are summarized in Tables I and II. These tables contain also the measured total M-shell x-ray production cross sections reported for $_1^1$H, $_2^3$He, and $_2^4$He ions for higher energies [36–38] as well as low-energy data for protons and deuterons [39–41]. Consequently, Tables I and II summarize the numerical results of total M-shell x-ray production cross sections for the hydrogen and helium ions' impact for the energy range 0.1–1.0 MeV/amu which was measured by our group [36–41]. Figure 7 shows the total M x-ray cross sections measured for gold for $_1^1$H, $_1^2$H, $_2^3$He, and $_2^4$He ions' impact in comparison with the theoretical predictions based on the PWBA, SCA, BEA, ECPSSR approaches, which are discussed in detail in the next section.

IV. THEORIES OF M-SHELL IONIZATION

For strongly asymmetric collisions ($Z_1 \ll Z_2$), such as the M-shell ionization of heavy atoms by light-, hydrogen, and helium ions' impact discussed here, the dominating process of inner-shell vacancy creation is Coulomb ionization, i.e., a

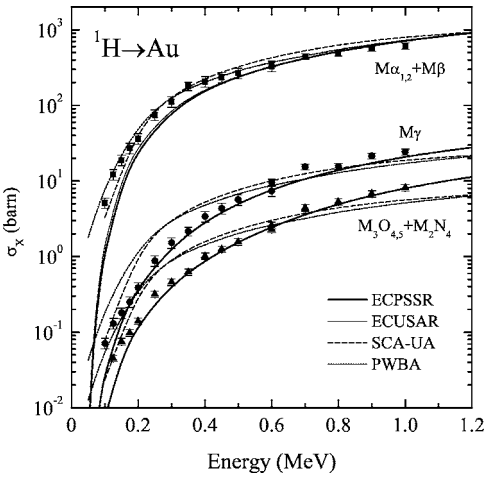

FIG. 5. The measured M x-ray production cross sections for gold bombarded by protons in the energy range 0.1–1.0 MeV for the following x-ray transitions: $M_{\alpha,\beta}(M_{4,5}N_{6,7})$, $M_\gamma(M_3N_{4,5})$, $M_3O_{4,5}+M_2N_4$, M_2O_4, and $M_1O_{2,3}$. The data are compared with prediction of PWBA, SCA-UA, ECPSSR, and ECUSAR approaches.

direct excitation of a single bound electron to the continuum by an incoming projectile (see, e.g., Ref. [94]). The other processes which can compete with direct ionization, namely the electron capture (EC) [95–98] to the projectile, the molecular excitation (MO) [99–105], and the recoil ionization (RI) [76,106–108], are negligible in this case. Similarly, the multiple ionization [109–111] and subshell coupling [79,85,86] effects play a minor role for the asymmetric collisions and thus the process of M-shell ionization by hydrogen and helium ions is expected to be solely described by the direct Coulomb ionization. The available theoretical approaches treating the direct ionization are based on the plane-

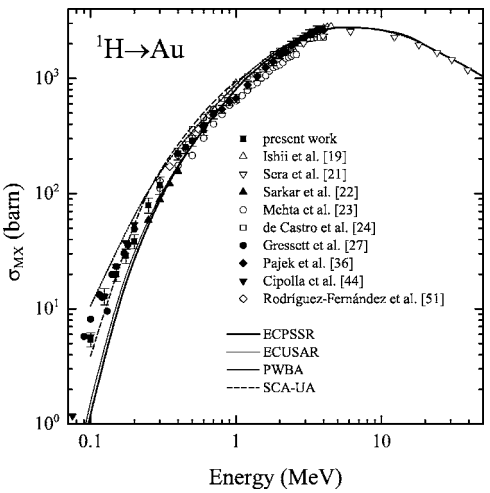

FIG. 6. A comparison of measured total M-shell x-ray production cross sections for Au bombarded by protons with the results available in the literature [19,21–24,27,36,44,51], which were obtained with the use of semiconductor x-ray detectors. The experimental results are compared with the theoretical predictions according to the PWBA, SCA-UA, ECPSSR, and ECUSAR approaches discussed in Sec. IV.

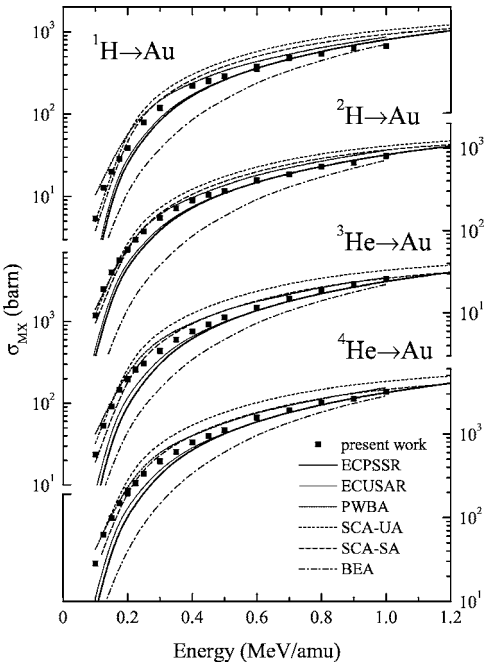

FIG. 7. Measured total M-shell x-ray production cross sections for gold bombarded by 0.1–1.0 MeV/amu $^1_1$H, $^2_1$H, $^3_2$He, and $^4_2$He ions. The data are compared with the predictions of the PWBA, ECPSSR, ECUSAR, SCA-SA, SCA-UA, and BEA approaches discussed in Sec. IV.

wave Born approximation (PWBA), the semiclassical approximation (SCA), and the binary-encounter approximation (BEA).

A. Plane-wave born approximation

The first theoretical attempts to describe the Coulomb ionization are related to the origins of quantum mechanics, namely a formulation of the Born approximation [112] and the first quantum-mechanical description of atomic collisions by Bethe [113], Mott [114], and Henneberg [115]. An application of the plane-wave Born approximation (PWBA) approach to the inner-shell ionization by heavy, charged particles was systematically presented by Merzbacher and Lewis [52]. The PWBA approach was further developed by Brandt and Lapicki [72,73] to include the effects which go beyond the first-order treatment, namely the binding polarization, Coulomb deflection, energy-loss, and relativistic effects, which is known as the ECPSSR theory [72,73]. The main dynamical scaling parameter ξ_i of the ECPSSR theory, which is proportional to the ratio of projectile and M-shell electron velocities, v_1 and $v_{M_i}=(2E_{M_i}/m_e)^{1/2}$, respectively, is defined as follows:

$$\xi_i = (2/\sqrt{\theta_i})v_1/v_{M_i}, \tag{1}$$

where $\theta_i=n^2E_{M_i}/Z_{M_i}^2\mathcal{R}$ is the outer screening constant, which is expressed by the electron binding energy E_{M_i} and the screened target atomic number Z_{M_i}, with n being the principal quantum number and $\mathcal{R}$ the Rydberg constant. According to the ECPSSR theory the ionization cross sections for M_i

subshell, $\sigma_{M_i}^{\mathrm{ECPSSR}}$ can be expressed in terms of the PWBA cross section, $\sigma_{M_i}^{\mathrm{PWBA}}(\xi_i,\theta_i)$, with appropriately modified scaling parameters $\xi_i \rightarrow \xi_i/\zeta_i$ and $\theta_i \rightarrow \zeta_i\theta_i$, where ζ_i is a dimensionless parameter describing an increase of the electron binding energy times the Coulomb deflection factor $C_i(x_i)$ and the energy-loss factor $f_i(z_i)$, namely (see Refs. [72,73])

$$\sigma_{M_i}^{\mathrm{ECPSSR}} = C_i(x_i) f_i(z_i) \sigma_{M_i}^{\mathrm{PWBA}}(\xi_i^R/\zeta_i, \zeta_i\theta_i). \tag{2}$$

The exact forms of ξ_i^R, ζ_i, x_i, and z_i quantities can be found in Refs. [72,73], however, their scaling properties will be discussed latter on in Sec. V in context of universal scaling of M-shell ionization cross sections and the isotopic effect. The nonrelativistic PWBA ionization cross sections for the M-shell reads [58]:

$$\sigma_{M_i}^{\mathrm{PWBA}}(\xi_i,\theta_i) = 8\pi a_0^2 (Z_1^2/Z_{M_i}^4) F_{M_i}(\xi_i,\theta_i)/\theta_i, \tag{3}$$

where the $F_{M_i}(\xi_i,\theta_i)$ functions were tabulated in Ref. [58] and a_0 is the Bohr radius. It is worth noting that for the M shell the θ_i parameter has nearly constant value and, additionally, for low energies ($\xi_i \ll 1$) the PWBA scaling function $F_{M_i}(\xi_i,\theta_i) \approx F_{M_i}(\xi_i)$ having the following limiting low-energy form [58,116]:

$$F_{M_i}(\xi_i) = \frac{(2j+1)2^{2\ell+6}}{(\ell+5)(2\ell+9)} \frac{n^4(n+\ell)!}{(n-\ell-1)!} \left(\frac{(n+\ell)}{(2\ell+1)!} \right)^2 \xi_i^{8+2\ell} \tag{4}$$

with (n,ℓ,j) denoting the quantum numbers of electron for the M_i subshell. Consequently, the ξ_i parameter is a very convenient quantity to demonstrate a universal scaling of the M-shell ionization cross sections. The discussed scaling properties of the PWBA and the ECPSSR approaches have been adopted to parametrize the empirical M-shell x-ray production cross sections for PIXE applications [40,41].

The ECPSSR theory has been recently modified by Lapicki *et al.* [74] to correct for the observed overestimation of the binding effect. In this approach, called the ECUSAR theory [74], the saturation of the corrected electron binding energy at its united atom (UA) limit value was proposed. Consequently, both the united and separated atom (USA) electron binding energies are reproduced in the ECUSAR theory. We note that for the asymmetric systems ($Z_1 \ll Z_2$) studied the predictions of M-shell ionization according to the ECPSSR and ECUSAR theories agree quite well, within 3%, for energies above 0.5 MeV/amu. For lower energies the predictions of the ECUSAR theory are systematically higher up to 25–50 % at 0.1 MeV/amu (see Fig. 8).

More detailed discussion of the effect of relativistic electronic wave functions on the M-shell ionization by protons in the energy range 0.06–2 MeV has been presented by Chen *et al.* [117–119]. These authors have tabulated the PWBA ionization cross sections calculated with the relativistic Dirac-Hartree-Slater wave functions (RPWBA-DHS) and using a correction [72] for the binding polarization and Coulomb deflection effects (RPWBA-DHS-BC) [119]. A comparison of relativistic (RPWBA-DHS) and nonrelativistic (PWBA-HS and PWBA-SH) ionization cross sections, obtained by using nonrelativistic Hartree-Slater (HS) and screened hydrogenic (SH) wave functions, can be found in Ref. [118]. Generally, the relativistic effects have only strong influence on ionization of the $M_{1,2,3}$ subshells, and consequently, they can be neglected for the total M-shell ionization cross sections dominated by ionization in the $M_{4,5}$ subshells [118]. In order to illustrate the effect of relativity on the M_i-subshell ionization by protons the relativistic RPWBA-DHS calculations [118] are compared in Fig. 9 with the nonrelativistic PWBA calculations with screened hydrogenic wave functions performed for gold atoms.

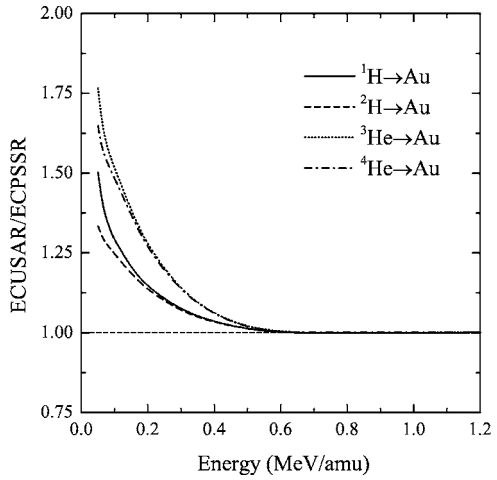

FIG. 8. The ratios of theoretical M-shell ionization cross sections for gold bombarded by $^1_1$H, $^2_1$H, $^3_2$He, and $^4_2$He ions calculated according to the ECUSAR and ECPSSR theories.

The *isotopic effect* expressing a dependence of the ionization cross sections on a mass of a given isotope, in addition to its velocity dependence, can be effectively applied to test the Coulomb deflection factor used in the ECPSSR theory, in particular, in the low velocity regime. In fact, a ratio of the ECPSSR ionization cross sections for a pair of isotopes with the same velocities, e.g., $^2_1$H/$^1_1$H or $^4_2$He/$^3_2$He, at low energies studied (0.1–1.0 MeV/amu) is determined by a ratio of corresponding Coulomb deflection factors due to the negligible role of the energy-loss factors. The Coulomb deflection factor used in the ECPSSR theory reads as follows [73,120]:

$$C_i(x_i) = \nu_i E_{\nu_i+1}[\pi d q_{oi} \zeta_i / z_i(1+z_i)], \tag{5}$$

where $E_{\nu_i}(\cdot)$ denotes the integral exponential function [121] of the order $\nu_i = 9 + 2\ell_i$, with ℓ_i being the orbital quantum number of electron. Here a minimum momentum transfer $q_{oi} = E_{M_i}/\hbar v_1$ and the half distance of closest approach in head-on collision $d = Z_1 Z_2 e^2/\mu v_1^2$, the latter depending on the reduced mass μ of the projectile-target atom system. In this way the isotopic effect appears in the ECPSSR ionization cross sections and thus the Coulomb deflection factor can be tested experimentally by comparing the measured M-shell ionization cross-section ratios, namely $\sigma(^2_1\mathrm{H})/\sigma(^1_1\mathrm{H})$ and $\sigma(^4_2\mathrm{He})/\sigma(^3_2\mathrm{He})$, at the same ion velocities, i.e., energy per mass, in particular for the low energies.

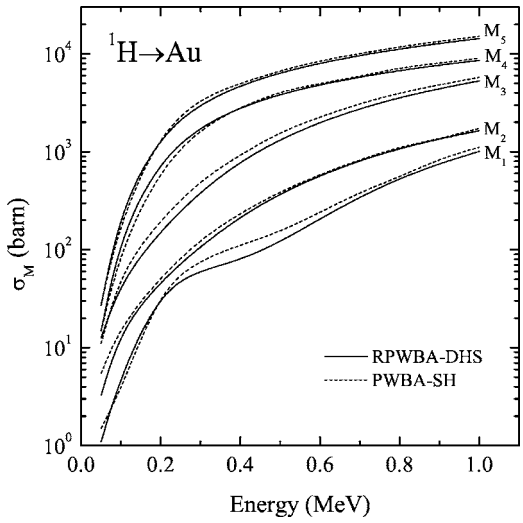

FIG. 9. Theoretical M_i-subshell ionization cross sections for gold bombarded by protons calculated using the PWBA approach with (i) the nonrelativistic screened hydrogenic wave functions (PWBA-SH) and (ii) with the relativistic Dirac-Hartree-Slater wave functions (RPWBA-DHS) [119]. A comparison of PWBA-SH and RPWBA-DHS calculations shows a role of the relativistic effects in *M*-shell ionization. Note a minor effect on the ionization of the $M_{4,5}$ subshell (*d* states).

B. Semiclassical approximation

The basic idea of application of the semiclassical approach in atomic collisions goes back to the works of Bohr, who formulated the so-called Bohr criterion [122] of a validity of a concept of classical trajectory. The semiclassical approximation (SCA) was formally further developed in connection with the nuclear Coulomb excitation [123] and then the SCA approach was applied by Bang and Hansteen [53] to the atomic processes, namely, a description of the inner-shell ionization by charged particles. A main assumption adopted in this approach is the validity of a concept of a classical projectile trajectory $\mathbf{R}(b,t)$, which parametrizes a position of the projectile moving in time t with an impact parameter b. For this reason the SCA approach is expected to be valid for the low-energy regime. The SCA amplitude for the excitation of an initially bound electron in a state $|\varphi_i\rangle$ to the final state $|E_f\rangle$ in the continuum can be obtained using the first-order time-dependent perturbation theory as follows:

$$a_{if}(b,E_f) = -\frac{i}{\hbar}\int_{-\infty}^{+\infty} dt e^{(i/\hbar)(E_f-E_i)t}\left\langle E_f\left|\frac{-Z_1e^2}{|\mathbf{r}-\mathbf{R}(b,t)|}\right|\varphi_i\right\rangle. \tag{6}$$

Finally, the total ionization cross section in the SCA approach is expressed by the following formula:

$$\sigma_{M_i}^{\mathrm{SCA}} = 2\pi\int_0^\infty bdb\left(\sum_{E_f}|a_{if}(b,E_f)|^2\right), \tag{7}$$

where the summation extends over possible electron final states $|E_f\rangle$ in the continuum. The SCA ionization cross sections for the straight-line trajectory and nonrelativistic hydrogenic wave functions for the *M* shell were tabulated by Hansteen *et al.* [60] (see also Refs. [59,61,62]). However, a more realistic description of the ionization process with the hyperbolic classical projectile trajectory and relativistic wave functions asks for advanced numerical SCA calculations (see, e.g., Refs. [62,76,78]).

For interpretation of the measured *M*-shell ionization cross sections the SCA calculations were performed following Eqs. (6) and (7). In these calculations, which are described in detail in Ref. [76], the hyperbolic projectile trajectories and hydrogenic relativistic electronic wave functions were used. The binding effect, caused by an increased electron binding energy due to a presence of the projectile in the vicinity of the target nucleus, was included in present SCA calculations in two extreme cases, namely the separated (SCA-SA) and united (SCA-UA) atom limits. Noting that a characteristic impact parameter, the so-called adiabatic radius $r_{ad}=\hbar v_1/E_{M_i}$, scales with the projectile velocity one expects that the SCA-UA approximation should describe the low-energy data, while for high energies the SCA-SA picture should be valid.

C. Binary-encounter approximation

A classical description of an ionization process was developed by Thomson [124] almost a century ago. This approach to the atomic collisions has been used to formulate the binary-encounter approximation (BEA) [125–128]. In this approach the ionization is treated as a classical collision of a projectile with free electron whose velocity distribution is given by the electronic wave function in the momentum space, in which the energy transferred exceeds the electron binding energy. A description of the inner-shell ionization by heavy particles was further elaborated within the BEA model by Garcia *et al.* [54] and others [55,129]. In general, the BEA model predicts a universal scaling of total ionization cross sections for arbitrary shell in terms of the relative projectile velocity $V=v_1/v_{M_i}$ as follows [55]:

$$\sigma_{M_i}^{BEA} = (N_i Z_1^2 \sigma_0/E_{M_i})G_i(V), \tag{8}$$

where N_i is a number of electrons in the shell and σ_0 can be found in Ref. [55]. The scaling function $G_i(V)$ was tabulated for different $n\ell$ states with $n\leqslant 2$ in Ref. [55]. Using the arguments of the Fock theorem [130], stating that a velocity distribution of electrons in a closed shell is the same as for the *s* state, the total BEA ionization cross sections for an arbitrary closed shell can be obtained using the scaling function for the *K* shell. In this way the *M*-shell ionization cross sections in the BEA model were obtained in the paper. We note, however, that the predictions of the classical BEA model are believed, in general, to be less precise than of alternative quantal PWBA and SCA approaches (see Fig. 10). The attempts to include in the BEA corrections for the Coulomb deflection, binding, and relativistic effects, which were undertaken for the *K* shell [131], were not convincing. For this reason, in the present work, more emphasis is put on a comparison of the experimental results with the PWBA and SCA approximations and the ECPSSR theory.

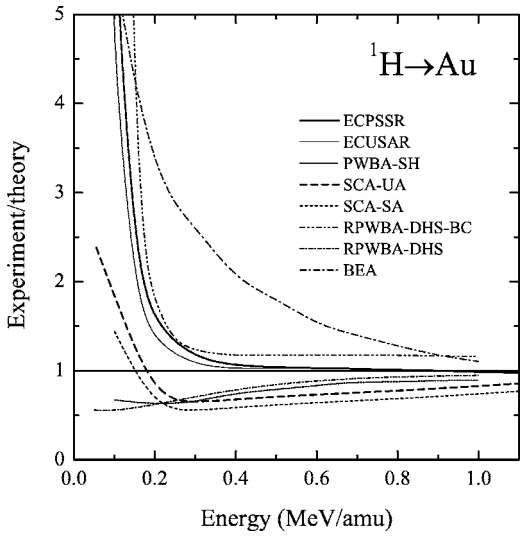

FIG. 10. Comparison of calculated and measured total M-shell ionization cross sections for protons on gold shown as experiment-to-theory ratios. The calculations were performed according to the following theoretical approaches: PWBA-SH, ECPSSR, ECUSAR, RPWBA-DHS, RPWBA-DHS-BC [119], SCA-SA, SCA-UA, and BEA, which are discussed in Sec. IV.

V. DISCUSSION

The understanding of the M x-ray production cross sections involves two aspects: first, a creation of a vacancy in the M shell and, second, a relaxation of the excited inner-shell state by emission of a photon. Consequently, the M-shell x-ray production cross section can be expressed as a product of the M-shell ionization cross section and the probability of x-ray emission, i.e., the M-shell fluorescence yield. The theories of M-shell ionization by charged particles have been discussed in Sec. IV, while the processes determining the emission of M x rays are discussed below.

A. *M* x-ray emission

An excited state of atom with a single vacancy in one of the M subshells can decay radiatively with emission of an x-ray photon, or nonradiatively, by emitting of an electron via the Auger, Coster-Kronig, or super-Coster-Kronig processes. In order to relate the M_i-subshell ionization cross sections σ_{M_i} with the x-ray production cross section σ_{M_i} for a given M x-ray transition $X_k(M_i)$, filling a vacancy in the M_i subshells, first, the vacancy *rearrangement* processes taking place prior to a moment of x-ray emission have to be taken into account. More precisely, a vacancy created at a moment of collision in the M_i subshell can be transferred to higher M_j subshell ($j>i$) via the Coster-Kronig or super-Coster-Kronig processes with a probability which is given by the corresponding (super-)Coster-Kronig yield f_{ij} [132]. Consequently, to account for the vacancy rearragement enhancing a number of vacancies in the subshell due to the (super-) Coster-Kronig transitions, the effective fluorescence yields ν_i are introduced (see Refs. [2,132]). With these quantities, the total M-shell x-ray production cross section σ_{MX} can be expressed as follows:

$$\sigma_{MX} = \sum_i \nu_i \sigma_{M_i}. \tag{9}$$

This equation can be used to calculate a theoretical total x-production cross section for the M shell. However, for testing different theoretical predictions of inner-shell ionization by ion impact it is more convenient to discuss the total M-shell ionization cross sections. For this reason, one introduces the effective M-shell fluorescence yield $\bar{\omega}_M$ relating the total x-ray production and ionization cross sections, namely

$$\sigma_{MX} = \bar{\omega}_M \sigma_M. \tag{10}$$

This relation defines the effective M-shell fluorescence yield $\bar{\omega}_M$ as follows:

$$\bar{\omega}_M = \sum_i w_i \nu_i, \tag{11}$$

where the weights w_i of the effective fluorescence yields ν_i are defined as $w_i = \sigma_{M_i}/\sigma_M$. It is important to note that the effective M-shell fluorescence yield $\bar{\omega}_M$ can be very well approximated (within 1%) by the following expression [36]:

$$\bar{\omega}_M \approx 0.4(\omega_4 + f_{45}\omega_5) + 0.6\omega_5. \tag{12}$$

This approximation is based on the fact that the weights w_i introduced in Eq. (11) can be well approximated by [0, 0, 0, 0.4, 0.6] (see Ref. [36]), which, in fact, reflects a dominating role of the $M_{4,5}$ subshells weighted by corresponding statistical weights. We note here that the approximate M-shell fluorescence yield $\bar{\omega}_M$ introduced by simple, nevertheless accurate, Eq. (12) allows one to derive the total M-shell ionization cross sections without earlier derivation of the M_i-subshell ionization cross sections. Consequently, by using Eqs. (10) and (12), the M-shell ionization cross sections can be obtained from the measured total M-shell x-ray production cross sections, namely $\sigma_M = \sigma_{MX}/\bar{\omega}_M$, to be further used to test the available theories for M-shell ionization by charged particles.

B. Scaling of *M*-shell ionization cross sections

The first-order theories of M-shell ionization by ion impact predict a common scaling of the ionization cross sections, namely $\sigma_{M_i} \propto (Z_1^2/Z_{M_i}^4)$. For instance, according to the PWBA approach [see Eq. (3)], the reduced M-shell ionization cross sections σ_M/σ_{0M}, with $\sigma_{0M} = 8\pi a_0^2 (Z_1^2/Z_M^4)$, are expected to scale in a universal way with dimensionless parameter $\xi_i \propto v_1/v_{M_i}$ [Eq. (1)], which describes a dynamics of the ionization process in the PWBA approach. A similar scaling of the reduced ionization cross sections with respect to the reduced velocity v_1/v_{M_i} can be expected for the SCA and BEA approaches. In spite of the higher-order effects as well as the Coulomb trajectory violating, in general, the scaling properties discussed above, the reduced ionization cross sections σ_M/σ_{0M} are expected to scale *approximately* with ξ_i, at least for a given ion impact. Such a scaling is justified by observing that the corrections for higher-order effects introduced in the ECPSSR theory depend mainly on scaled ve-

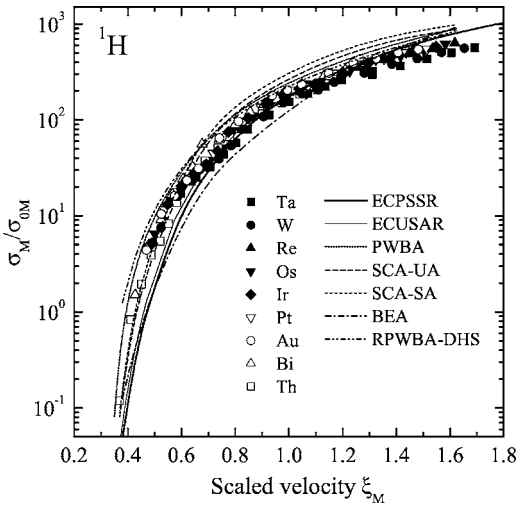

FIG. 11. The measured *M*-shell ionization cross sections for protons in the energy range 0.1–1.0 MeV/amu plotted as the reduced ionization cross sections σ_M/σ_{0M}, with $\sigma_{0M}=8\pi a_0^2(Z_1^2/Z_M^4)$, versus the scaled velocity parameter $\xi_i \propto v_1/v_{M_i}$ [Eq. (1)]. The targets studied are shown in the figure. The data are compared with the predictions of the PWBA, RPWBA-DHS, ECPSSR, ECUSAR, SCA-SA, SCA-UA, and BEA calculations, which are discussed in Sec. IV.

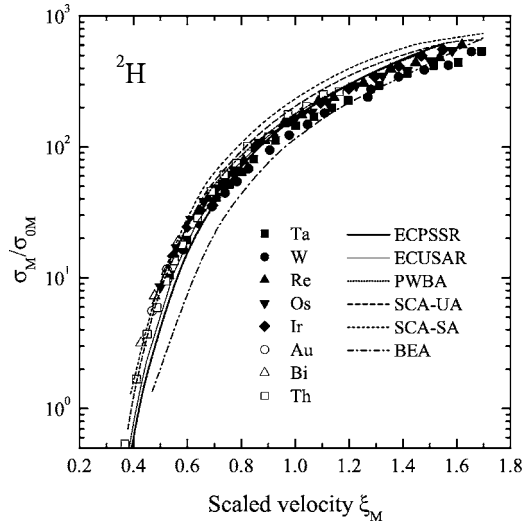

FIG. 12. The same as in Fig. 11, but for $^2_1$H ions.

locity ξ_i and the projectile type, via its atomic number Z_1 and a reduced mass of the colliding system $\mu=M_1M_2/(M_1+M_2)$, which for asymmetric collisions discussed $\mu \approx M_1$. More precisely, following Refs. [72,73] one finds $\zeta_i(Z_1,\xi_i)$, $x_i(Z_1/\mu,\xi_i)$, $z_i(\mu,\xi_i)$, and $\xi_i^R(\xi_i)$, which supports the idea of approximate universal scaling of ionization cross sections for a given projectile (Z_1,M_1). This scaling gives a possibility to present the systematic results of *M*-shell ionization for different elements in a unified and convenient way, in particular, with respect to comparison to the theoretical predictions. The measured reduced ionization cross sections for the *M* shell for studied elements are shown in Figs. 11–14 for incident $^1_1$H, $^2_1$H, $^3_2$He, and $^4_2$H ions, respectively, in the energy range 0.1–1.0 MeV/amu. In fact, the experimental data for the *M* shell support the scaling of ionization cross sections for a given ion impact for all elements studied from Ta to Th.

The measured *M*-shell ionization cross sections are compared in Figs. 11–14 with the theoretical predictions which were obtained using different approaches discussed, namely the PWBA, ECPSSR, SCA, and BEA. Additionally, the predictions of relativistic RPWBA-DHS calculations for proton impact are shown in Fig. 11. In general, the data support the universal scaling of measured cross sections with scaled velocity parameter $\xi_i \propto v_1/v_{M_i}$ [Eq. (1)]. The existing discrepancies are related, in our opinion, to the description of the binding effect, which is clearly observed by comparing the SCA-SA and SCA-UA calculations [75–77] treating two extreme situations of separated (SA) and united (UA) atoms in the collision. A role of the Coulomb deflection effect is demonstrated by comparing the theoretical predictions using straight-line trajectories (PWBA [58], SCA of Hansteen *et al.* [60], BEA [55,129]), modeling the Coulomb deflection effect (ECPSSR [72,73] and RPWBA-DHS-BC [119]) and, finally, using exact hyperbolic trajectories in calculations (SCA-SA and SCA-UA [75–77]). In particular, the Coulomb deflection effect seems to be overestimated by the ECPSSR theory, which is observed for very low projectile energies. The relativistic effects seem to be less important for discussed *total* *M*-shell ionization cross sections (cf. RPWBA-DHS and PWBA calculations for protons), which was discussed in detail by Chen [118].

It is interesting to note that the scaling of the *M*-shell ionization cross sections discussed above can be extended to the *M* x-ray production cross sections, which is of practical importance for PIXE applications. As we have shown earlier [40,41], by combining the facts that (i) the M_i-subshell radiative widths scale with screened target atomic number as $Z_{M_i}^4$ and thus *approximately* the M_i-subshell fluorescence yields $\omega_{M_i} \propto Z_{M_i}^4$ and (ii) that the ionization cross sections $\sigma_{M_i} \propto Z_{M_i}^{-4}$ [see Eq. (3)], one proves the universal scaling of *M* x-ray production cross sections with respect to the scaled velocity $\xi_i \propto v_1/v_{M_i}$ [Eq. (1)]. Such a scaling of the *M* x-ray production cross sections for protons and deuterons has been

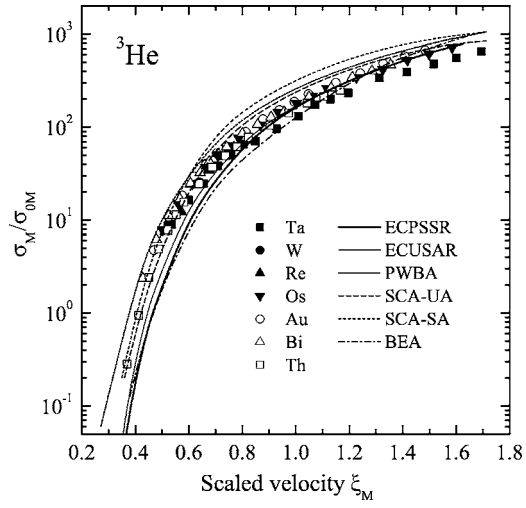

FIG. 13. The same as in Fig. 11, but for $^3_2$He ions.

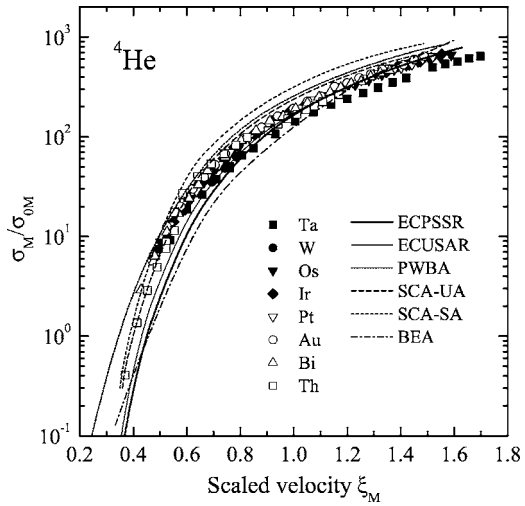

FIG. 14. The same as in Fig. 11, but for $^4_2$He ions.

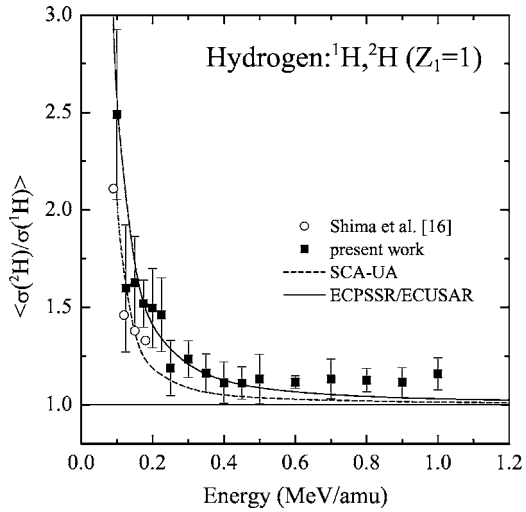

FIG. 15. The averaged ratios of measured total M-shell ionization cross sections $\sigma(^2_1\mathrm{H})/\sigma(^1_1\mathrm{H})$, plotted versus the energy per atomic mass unit, showing a magnitude of the isotopic effect. The cross-section ratios measured by Shima *et al.* [16] for tungsten are also shown in the figure. The corresponding ratios of the theoretical cross sections according to the ECPSSR and ECUSAR, which practically coincide, and SCA-UA calculations are shown in the figure.

discussed in detail in Refs. [40,41] in the context of the derivation of accurate empirical x-ray cross sections for the M shell for PIXE applications and thus it will not be discussed here.

C. Isotopic effect

The systematic experimental data concerning the M-shell ionization by the, $^1_1$H, $^2_1$H, $^3_2$He, and $^4_2$H ions, measured at equal-velocity conditions, in the energy range 0.1–1.0 MeV/amu (see Tables I and II) offer a possibility to verify a description of the Coulomb deflection effect proposed within the ECPSSR theory. This is, in particular, a case when the predictions of the ECPSSR theory, which treats the Coulomb trajectory effect in a form of a multiplicative factor $C(x_i) \approx \nu_i \exp(-x_i)/(x+\nu_i+1)$ [see Eq. (5) and Refs. [73,120,121]], can be compared with the results of the SCA calculations [75–77] using exact hyperbolic trajectories for the limiting separated (SA) and united (UA) atoms cases. Taking into account that the energy-loss effect does not play an important role ($z_i \approx 1$) for studied energies, one finds that for asymmetric collision ($M_1 \ll M_2$) the argument of the Coulomb deflection factor $x_i \propto Z_1/M_1$. This means that a magnitude of the Coulomb deflection factor used in the ECPSSR theory is expected to be very different for low-velocity light projectiles such as $^1_1$H, $^2_1$H, $^3_2$He, and $^4_2$He, for which the Z_1/M_1 ratios are 1, 1/2, 2/3, and 1/2, respectively. In order to verify experimentally the Coulomb deflection factor used in the ECPSSR theory the ratios of M-shell ionization cross sections for the pair of isotopes with the same velocities, namely $\sigma(^2_1\mathrm{H})/\sigma(^1_1\mathrm{H})$ and $\sigma(^4_2\mathrm{He})/\sigma(^3_2\mathrm{He})$, averaged over studied target atoms are compared in Figs. 15 and 16 with the predictions of the ECPSSR theory and the SCA calculations. Additionally, in Fig. 15 the $\sigma(^2_1\mathrm{H})/\sigma(^1_1\mathrm{H})$ ratios measured by Shima *et al.* [16] are shown, being the only results available for the discussed ratios reported by others. We note that these ratios are in good agreement with the present data. The ratios of measured ionization cross sections for two isotopes for the same ion velocities, i.e., the same ξ, namely $\sigma(^2_1\mathrm{H})/\sigma(^1_1\mathrm{H})$ and $\sigma(^4_2\mathrm{He})/\sigma(^3_2\mathrm{He})$, are equal, within the ECPSSR theory [see Eq. (2)], approximately to the ratios of corresponding Coulomb deflection factors $C(Z_1/M_1, \xi_i)$. On the other hand, the corresponding cross-section ratios calculated using the SCA theory with exact Coulomb hyperbolic trajectories show exact values of the isotopic effect and thus can be used to test the Coulomb deflection factor used in the ECPSSR theory. Such a comparison, shown in Figs. 15 and 16 indicates rather good agreement between the predictions of the ECPSSR and the SCA calculations, suggesting that a general deficiency of the ECPSSR theory in describing the low-energy data (see Figs. 11–14) can be related to the binding effect.

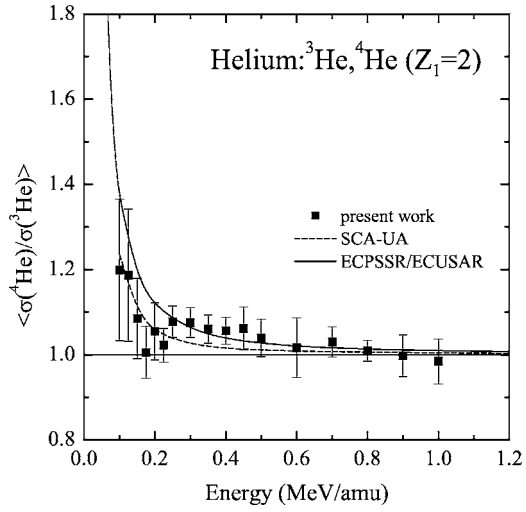

FIG. 16. The same as in Fig. 15, but for $\sigma(^4_2\mathrm{He})/\sigma(^3_2\mathrm{He})$ cross-section ratios.

D. Electron binding effect

A systematic comparison of measured *M*-shell ionization cross sections for $^1_1$H, $^2_1$H, $^3_2$He, and $^4_2$He ions in the energy range 0.1–1.0 MeV/amu with the predictions of the ECPSSR and SCA calculations (see Figs. 11–16) suggests that observed systematic underestimation of the data by the ECPSSR theory at low energies can be related to the overestimation of the binding effect in this theory. In fact, the parameter $\zeta_i(Z_1,\xi_i)$, which describes in the ECPSSR theory the binding effect, i.e., an increase of the electron binding energy due to the presence of a projectile in the vicinity of the target atom nucleus, for the *extreme adiabatic* regime $\xi_i \simeq 0$ has the following form [72]:

$$\zeta_i(\xi_i = 0) = 1 + 2Z_1/\theta_i Z_{M_i}. \tag{13}$$

This formula does not meet the physically expected value for the ratio of electron binding energies in the united atom, $E_{M_i}(Z_1+Z_2)$, and separated atom, $E_{M_i}(Z_2)$, limits, namely

$$E_{M_i}(Z_1 + Z_2)/E_{M_i}(Z_2) \simeq (1 + Z_1/Z_{M_i})^2. \tag{14}$$

By comparing Eqs. (13) and (14) one finds immediately that at least in the adiabatic regime the electron binding effect is systematically overestimated (3–7 %) in terms of the $\zeta_i(\xi_i=0)$ parameter. Moreover, taking into account that at very low energies the ECPSSR *M*-shell ionization cross sections scale with very high power of ζ_i, namely as $\sigma^{\mathrm{ECPSSR}}_{M_i} \propto 1/\zeta_i^{13}$ [see Eqs. (3) and (4)] for dominating $M_{4,5}$ subshells (*d* states with $\ell=2$), one arrives at almost a factor of 2 underestimation of the ionization cross sections in the adiabatic regime ($\xi_i \approx 0$) by the ECPSSR theory due to an overestimation of the binding effect in this approach.

In order to demonstrate this observation the ratios of the reduced *M*-shell ionization cross sections $\bar{\sigma}=\sigma_M/\sigma_{0M}$ measured for the $^4_2$He and $^2_1$H ions, averaged over studied target atoms, are plotted in Fig. 17 versus the energy per atomic units. In fact, using the theoretical arguments from a discussion of the isotopic effect given above, one finds that for the $^4_2$He and $^2_1$H ions considered here the Coulomb deflection factors $C(Z_1/M_1,\xi_i)$ used in the ECPSSR theory should cancel out due to the same charge-to-mass ratio (1/2) for these ions. On the other hand, a remaining dependence of the $\zeta_i(Z_1,\xi_i)$ parameter on the projectile atomic number Z_1 makes this ratio sensitive on the binding effect correction in the ECPSSR theory. Consequently, a suggested overestimation of the binding correction in the ECPSSR theory would result in smaller values of the theoretical $\bar{\sigma}(^4_2\mathrm{He})/\bar{\sigma}(^2_1\mathrm{H})$ ratios with respect to the measured ones, in particular for the low energies. Indeed, this effect is clearly visible in Fig. 17, supporting thus a suggestion of overestimation of the binding correction in the ECPSSR theory. On the other hand, an overestimation of the effective electron binding energy in the ECPSSR theory was corrected for in the recent ECUSAR theory [74] in which the saturation of the binding energy at the united atom value was introduced. The $\bar{\sigma}(^4_2\mathrm{He})/\bar{\sigma}(^2_1\mathrm{H})$ ratios, being sensitive predominantly on the binding correction used due to cancellation of the Coulomb deflection factors for the same charge-to-mass ratio ions, are well reproduced by the predictions of the ECUSAR theory [see Fig. 17]. However, despite this improvement the absolute values of the ECPSSR/ECUSAR calculations remain systematically smaller, by a factor of 3–5, than the experimental *M*-shell ionization cross sections for the lowest energies for studied ions. This discrepancy, which could be related to more fundamental limitations of the approximations used in the ECPSSR/ECUSAR approaches which do not manifest themselves in the cross section ratios discussed here, needs further studies to be explained in detail.

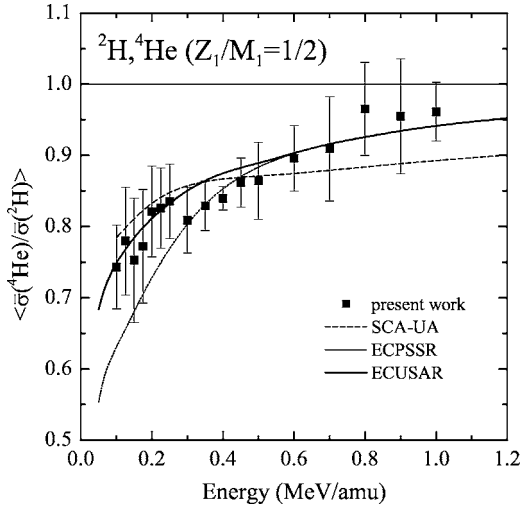

FIG. 17. The averaged ratios of measured reduced *M*-shell ionization cross sections $\bar{\sigma}(^4_2\mathrm{He})/\bar{\sigma}(^2_1\mathrm{H})$, where $\bar{\sigma}=\sigma_M/\sigma_{0M}$ with $\sigma_{0M}=8\pi a_0^2(Z_1^2/Z_M^4)$, plotted versus the energy per atomic mass unit showing a role of the binding correction in the ECPSSR theory. The corresponding ratios of the theoretical cross sections according to the ECPSSR and ECUSAR theories and SCA-UA calculations are shown in the figure.

VI. CONCLUSIONS

The *M*-shell ionization by light $^1_1$H, $^2_1$H, $^3_2$He, and $^4_2$He ions in the energy range 0.1–1.0 MeV/amu has been systematically studied for selected heavy elements (Ta–Th) covering the atomic number range $Z_2=73-90$. Derived *reduced* *M*-shell ionization cross sections σ_M/σ_{0M} exhibit a universal scaling, for a given projectile, with respect to the scaled velocity $\xi_i \propto v_1/v_{M_i}$. This property offers a good way to obtain the accurate *empirical* *M*-shell ionization, or *M* x-ray production, cross sections to be used in PIXE applications. On the other hand, the measured data were used to verify the existing theoretical predictions of *M*-shell ionization by charged particles, which are based on the PWBA, SCA, and BEA approaches as well as their modifications including the higher-order effects (ECPSSR, RPWBA-DHS-BC, SCA-UA). In particular, a systematic character of the present data allowed us to study the *isotopic effect* by comparing the $\sigma(^2_1\mathrm{H})/\sigma(^1_1\mathrm{H})$ and $\sigma(^4_2\mathrm{He})/\sigma(^3_2\mathrm{He})$ ratios, measured for equal-velocity projectiles, with the predictions of the ECPSSR and the SCA calculations. We have found in this way that the ECPSSR theory describes reasonably well the Coulomb deflection effect. On the other hand, the observed

systematic underestimation of the *M*-shell ionization cross sections by the ECPSSR theory at very low energies is attributed, in our opinion, to inadequate description of the *binding effect* in this approach. The recent ECUSAR theory, despite containing the saturation of binding effect, still systematically underestimates the *M*-shell data for low energies, similarly as the ECPSSR theory. This systematic deficiency of the ECPSSR/ECUSR approaches for very low projectile velocities has to be further investigated. Finally, the present results give some interesting arguments to improve the existing theories of *M*-shell ionization by charged particles, however, this task is out of the scope of the present paper. We also note that the reported data substantially extend the *M*-shell ionization cross-section data basis for PIXE applications.

ACKNOWLEDGMENTS

This work was supported by the Polish State Committee for Scientific Research (KBN) under Grant Nos. 5P03B-11420 and 2P03B-03824. We would like to express our thanks to the staff of the 3-MeV Van de Graaff accelerator at the SINS, Warsaw, for their contribution to this work.

[1] J. Garcia, R. Fortner, and T. Kavanagh, Rev. Mod. Phys. **45**, 111 (1973).
[2] W. Bambynek, B. Crasemann, R. Fink, H.-U. Freund, H. Mark, C. Swift, R. Price, and P. V. Rao, Rev. Mod. Phys. **44**, 716 (1972).
[3] C. H. Rutlege and R. L. Watson, At. Data Nucl. Data Tables **12**, 197 (1973).
[4] T. L. Hardt and R. L. Watson, At. Data Nucl. Data Tables **17**, 107 (1976).
[5] R. K. Gardner and T. J. Gray, At. Data Nucl. Data Tables **21**, 515 (1978).
[6] R. S. Sokhi and D. Crumpton, At. Data Nucl. Data Tables **30**, 49 (1984).
[7] H. Paul and J. Muhr, Phys. Rep. **135**, 47 (1986).
[8] G. Lapicki, J. Phys. Chem. Ref. Data **18**, 111 (1989).
[9] I. Orlić, C. H. Sow, and S. M. Tang, At. Data Nucl. Data Tables **56**, 59 (1994).
[10] P. Needham and B. Sartwell, Phys. Rev. A **2**, 27 (1970).
[11] G. Bissinger, P. H. Nettles, S. M. Shafroth, and A. W. Waltner, Phys. Rev. A **10**, 1932 (1974).
[12] R. Jopson, H. Mark, and D. Swift, Phys. Rev. **127**, 1612 (1962).
[13] J. Khan, D. Potter, and D. Worley, Phys. Rev. **135**, A511 (1964).
[14] J. Khan, D. Potter, and D. Worley, Phys. Rev. **139**, A1735 (1965).
[15] P. Needham and B. Sartwell, Phys. Rev. A **2**, 1686 (1970).
[16] K. Shima, I. Makino, and M. Sakisaka, J. Phys. Soc. Jpn. **30**, 611 (1971).
[17] C. Busch, A. Bashkin, P. Nettles, S. Shafroth, and A. Waltner, Phys. Rev. A **7**, 1601 (1973).
[18] S. Thornton, R. McKnight, and R. Karlowicz, Phys. Rev. A **10**, 219 (1974).
[19] K. Ishii, S. Morita, H. Tawara, H. Kaji, and T. Shiokawa, Phys. Rev. A **11**, 119 (1975).
[20] M. Poncet and C. Engelmann, Nucl. Instrum. Methods **159**, 455 (1979).
[21] K. Sera, K. Ishii, A. Yamadera, A. Kuwako, M. Kamiya, M. Sebata, S. Morita, and T. Chu, Phys. Rev. A **22**, 2536 (1980).
[22] M. Sarkar, H. Mommsen, W. Sarter, and P. Schürkes, J. Phys. B **14**, 3163 (1981).
[23] R. Mehta, J. Duggan, J. Price, F. McDaniel, and G. Lapicki, Phys. Rev. A **26**, 1883 (1982).
[24] N. de Castro Faria, J. F. L. Freire, A. de Pinho, and E. da Silveira, Phys. Rev. A **28**, 2770 (1983).
[25] R. Mehta, J. Duggan, J. Price, P. Kocur, F. McDaniel, and G. Lapicki, Phys. Rev. A **28**, 3217 (1983).
[26] R. Gowda and D. Powers, Phys. Rev. A **31**, 134 (1985).
[27] J. Gressett, D. Marble, F. McDaniel, J. Duggan, J. Culwell, and G. Lapicki, Nucl. Instrum. Methods Phys. Res. B **40/41**, 116 (1989).
[28] A. Jesus and J. Ribeiro, Nucl. Instrum. Methods Phys. Res. A **280**, 370 (1989).
[29] R. Mehta, J. L. Duggan, F. D. McDaniel, M. C. Andrews, G. Lapicki, P. D. Miller, L. A. Rayburn, and A. R. Zander, Phys. Rev. A **28**, 2722 (1983).
[30] M. C. Andrews, F. D. McDaniel, J. L. Duggan, P. D. Miller, P. L. Pepmiller, H. F. Krause, T. M. Rosseel, L. A. Rayburn, R. Mehta, and G. Lapicki, Phys. Rev. A **36**, 3699 (1987).
[31] J. Price, J. L. Duggan, F. D. McDaniel, G. Lapicki, and R. Mehta, Phys. Rev. A **37**, 365 (1988).
[32] Y. Yu, H. Sun, J. L. Duggan, F. D. McDaniel, J. Yin, and G. Lapicki, Phys. Rev. A **52**, 3836 (1995).
[33] T. Czyżewski *et al.*, Nucl. Instrum. Methods Phys. Res. B **109/110**, 52 (1996).
[34] D. Mitra, M. Sarkar, D. Bhattacharya, P. Sen, and G. Kuri, Nucl. Instrum. Methods Phys. Res. B **145**, 283 (1998).
[35] M. Pajek, A. P. Kobzev, R. Sandrik, R. A. Ilkhamov, and S. H. Khusmurodov, Nucl. Instrum. Methods Phys. Res. B **42**, 346 (1989).
[36] M. Pajek, A. Kobzev, R. Sandrik, A. Skrypnik, R. Ilkhamov, S. Khusmurodov, and G. Lapicki, Phys. Rev. A **42**, 261 (1990).
[37] M. Pajek, A. Kobzev, R. Sandrik, A. Skrypnik, R. Ilkhamov, S. Khusmurodov, and G. Lapicki, Phys. Rev. A **42**, 5298 (1990).
[38] M. Pajek, A. Kobzev, R. Sandrik, A. Skrypnik, R. Ilkhamov, S. Khusmurodov, and G. Lapicki, Phys. Rev. A **42**, 6582 (1990).
[39] A. Bieńkowski, J. Braziewicz, T. Czyżewski, L. Głowacka, M. Jaskóła, G. Lapicki, and M. Pajek, Nucl. Instrum. Methods Phys. Res. B **49**, 19 (1990).
[40] M. Pajek, M. Jaskóła, T. Czyżewski, L. Głowacka, D. Banaś, J. Braziewicz, W. Kretschmer, G. Lapicki, and D. Trautmann, Nucl. Instrum. Methods Phys. Res. B **150**, 33 (1999).
[41] M. Jaskóła, T. Czyżewski, L. Głowacka, D. Banaś, J. Braziewicz, M. Pajek, W. Kretschmer, G. Lapicki, and D. Trautmann, Nucl. Instrum. Methods Phys. Res. B **161**, 191 (2000).

[42] H. Sun, J. Kirchoff, A. Azordegan, J. L. Duggan, F. D. McDaniel, R. Wheeler, R. Chaturvedi, and G. Lapicki, Nucl. Instrum. Methods Phys. Res. B **79**, 186 (1993); **79**, 194 (1993).
[43] X. Cai, Z. Liu, X. Chen, S. Ma, Z. Chen, Q. Xu, H. Liu, and X. Ma, Phys. Scr. **47**, 751 (1993).
[44] S. Cipolla, Nucl. Instrum. Methods Phys. Res. B **99**, 22 (1995).
[45] F. Shokouhi, S. Fazinić, I. Bogdanović, M. Jakšić, V. Valković, and H. Afarideh, Nucl. Instrum. Methods Phys. Res. B **109/110**, 15 (1996).
[46] J. Braich, P. Verma, H. Verma, D. Goyal, A. Mandl, B. Dhal, H. Padhi, and H. Verma, Nucl. Instrum. Methods Phys. Res. B **119**, 317 (1996).
[47] J. Braich, P. Verma, and H. Verma, J. Phys. B **30**, 2359 (1997).
[48] A. Amirabadi, H. Afarideh, S. Haji-Saeid, F. Shokouhi, and H. Peyrovan, J. Phys. B **30**, 863 (1997).
[49] S. Cipolla, P. Teeter, and J. McClure, in *Application of Accelerators in Research and Industry*, edited by J. L. Duggan and I. L. Morgan, AIP Conf. Proc. No. 475 (AIP, Woodbury, NY, 1999), p. 36.
[50] K. Welsh and S. Cipolla, in *Application of Accelerators in Research and Industry* (Ref. [49]), p. 23.
[51] L. Rodriguez-Fernández, J. Miranda, J. Ruvalcaba-Sil, E. Segundo, and A. Olivier, Nucl. Instrum. Methods Phys. Res. B **189**, 27 (2002).
[52] R. Merzbacher and H. W. Lewis, *Handbuch der Physik*, edited by Flügge (Springer, Berlin, 1958), Vol. 34, p. 166.
[53] J. Bang and J. M. Hansteen, K. Dan. Vidensk. Selsk. Mat. Fys. Medd. **31**, No. 13 (1959).
[54] J. Garcia, Phys. Rev. A **1**, 280 (1970); **1**, 1402 (1970).
[55] J. McGuire and P. Richard, Phys. Rev. A **8**, 1374 (1973).
[56] B. H. Choi, E. Merzbacher, and G. S. Khandelwal, At. Data **5**, 291 (1973).
[57] R. Rice, G. Basbas, and F. D. McDaniel, At. Data Nucl. Data Tables **20**, 503 (1977).
[58] D. E. Johnson, G. Basbas, and F. D. McDaniel, At. Data Nucl. Data Tables **24**, 1 (1979).
[59] J. M. Hansteen and O. P. Mosebekk, Nucl. Phys. A **201**, 541 (1973).
[60] J. M. Hansteen, O. M. Johnsen, and L. Kocbach, At. Data Nucl. Data Tables **15**, 305 (1975).
[61] J. M. Hansteen, Adv. At. Mol. Phys. **11**, 299 (1975).
[62] L. Kocbach, J. Phys. B **9**, 2269 (1976).
[63] R. W. Brandt and I. Sellin, Phys. Rev. **151**, 56 (1966).
[64] A. Amundsen, J. Phys. B **10**, 2177 (1977).
[65] M. Pauli and D. Trautmann, J. Phys. B **11**, 667 (1978).
[66] D. Jamnik and Č. Zupancič, K. Dan. Vidensk. Selsk. Mat. Fys. Medd. **31**, No. 2 (1957).
[67] B. H. Choi, Phys. Rev. A **4**, 1002 (1971).
[68] P. Amundsen and L. Kocbach, J. Phys. B **8**, L122 (1975).
[69] M. Pauli, F. Rösel, and D. Trautmann, J. Phys. B **11**, 2511 (1978).
[70] G. Basbas, W. Brandt, and R. Laubert, Phys. Rev. A **7**, 983 (1973).
[71] W. Brandt and G. Lapicki, Phys. Rev. A **10**, 474 (1974).
[72] W. Brandt and G. Lapicki, Phys. Rev. A **20**, 465 (1979).
[73] W. Brandt and G. Lapicki, Phys. Rev. A **23**, 1717 (1981).
[74] G. Lapicki, G. A. V. R. Murty, G. J. N. Raju, B. S. Reddy, S. B. Reddy, and V. Vijayan, Phys. Rev. A **70**, 062718 (2004).
[75] D. Trautmann and F. Rösel, Nucl. Instrum. Methods **169**, 259 (1980).
[76] D. Trautmann, F. Rösel, and G. Baur, Nucl. Instrum. Methods Phys. Res. **214**, 21 (1983).
[77] D. Trautmann and T. Kauer, Nucl. Instrum. Methods Phys. Res. B **42**, 449 (1989).
[78] Z. Halabuka, W. Preger, and D. Trautmann, Z. Phys. D: At., Mol. Clusters **29**, 151 (1994).
[79] L. Sarkadi and T. Mukoyama, J. Phys. B **14**, L255 (1981).
[80] M. H. Martir, A. L. Ford, J. F. Reading, and R. L. Becker, J. Phys. B **15**, 2405 (1982).
[81] G. Mehler, T. De Reus, U. Müller, J. Reinhardt, B. Müller, W. Greiner, and G. Soff, Nucl. Instrum. Methods Phys. Res. A **240**, 559 (1987).
[82] L. Sarkadi, J. Phys. B **19**, L755 (1986).
[83] L. Sarkadi and T. Mukoyama, J. Phys. B **20**, L559 (1987).
[84] L. Sarkadi and T. Mukoyama, J. Phys. B **23**, 3849 (1990).
[85] L. Sarkadi, T. Mukoyama, and Ž. Šmit, J. Phys. B **29**, 2253 (1996).
[86] M. Pajek *et al.*, Phys. Rev. A **68**, 022705 (2003).
[87] J. Marion, Rev. Mod. Phys. **38**, 660 (1966).
[88] H. Paul and O. Bolik, At. Data Nucl. Data Tables **54**, 75 (1993).
[89] E. Huttel, W. Arnold, H. Baumgart, and G. Clausnitzer, Nucl. Instrum. Methods Phys. Res. B **12**, 193 (1985).
[90] W. Mehlhorn, Phys. Lett. **26**, 166 (1968).
[91] V. Sizov and N. Kabachnik, J. Phys. B **13**, 1601 (1980).
[92] J. Wigger, H. Altevogt, M. Brüssermann, G. Richter, and B. Cleff, J. Phys. B **17**, 4741 (1984).
[93] T. Blümke, W. Meierkord, H.-U. Menzebach, J. Pennins, Z. Stachura, W. Vollmer, and B. Cleff, Z. Phys. D: At., Mol. Clusters **21**, 131 (1991).
[94] P. Mokler and F. Folkmann, *Structure and Collisions of Ions and Atoms*, edited by I. A. Sellin (Springer, Berlin, 1978), p. 201.
[95] J. Oppenheimer, Phys. Rev. **31**, 349 (1928).
[96] H. Brinkmann and H. Kramers, Proc. R. Acad. Sci. Amsterdam **33**, 973 (1930).
[97] V. Nikolaev, Zh. Eksp. Teor. Fiz. **51**, 1263 (1966) [Sov. Phys. JETP **24**, 847 (1967)].
[98] G. Lapicki and F. McDaniel, Phys. Rev. A **22**, 1896 (1980).
[99] M. Born and J. Oppenheimer, Ann. Phys. **84**, 457 (1927).
[100] U. Fano and W. Lichten, Phys. Rev. Lett. **14**, 627 (1965).
[101] M. Bara and W. Lichten, Phys. Rev. A **6**, 211 (1972).
[102] J. Briggs, J. Phys. B **18**, L485 (1975).
[103] J. Briggs, Rep. Prog. Phys. **39**, 217 (1976).
[104] W. Lichten, J. Phys. Chem. **84**, 2102 (1980).
[105] U. Wille and R. Hippler, Phys. Rep. **132**, 129 (1986).
[106] A. Migdal, J. Phys. (Moscow) **4**, 449 (1941).
[107] M. Kleber and K. Unterseer, Z. Phys. A **292**, 311 (1979).
[108] F. Rösel, D. Trautmann, and G. Baur, Nucl. Instrum. Methods Phys. Res. **192**, 43 (1982).
[109] J. M. Hansteen and O. P. Mosebekk, Phys. Rev. Lett. **29**, 1361 (1972).
[110] J. H. McGuire and P. Richard, Phys. Rev. A **8**, 1374 (1973).
[111] B. Sulik, G. Hock, and D. Berényi, J. Phys. B **17**, 3239 (1984).
[112] M. Born, Z. Phys. **38**, 803 (1926).
[113] H. Bethe, Ann. Phys. **5**, 325 (1930).
[114] N. Mott, Proc. Cambridge Philos. Soc. **27**, 553 (1931).

[115] W. Henneberg, Z. Phys. **86**, 592 (1933).
[116] E. Montenegro and A. de Pinho, J. Phys. B **15**, L275 (1982).
[117] M. H. Chen, B. Crasemann, and H. Mark, Phys. Rev. A **27**, 2358 (1983).
[118] M. H. Chen, Phys. Rev. A **30**, 2082 (1984).
[119] M. H. Chen, Phys. Rev. A **40**, 2758 (1989).
[120] G. Lapicki, M. Goldstein, and W. Brandt, Phys. Rev. A **23**, 2727 (1981).
[121] M. Abramowitz and I. Stegun, *Handbook of Mathematical Functions* (Dover, New York, 1965).
[122] N. Bohr, K. Dan. Vidensk. Selsk. Mat. Fys. Medd. **18**, No. 8 (1948).
[123] K. Alder, A. Bohr, T. Huus, B. Mottelson, and A. Winther, Rev. Mod. Phys. **28**, 432 (1956).
[124] J. Thomson, Philos. Mag. **23**, 449 (1912).
[125] M. Gryzinski, Phys. Rev. **138**, A305 (1965); **138**, A322 (1965); **138**, A336 (1965).
[126] E. Gerjuoy, Phys. Rev. **148**, 54 (1966).
[127] L. Vriens, Proc. Phys. Soc. London **90**, 935 (1966).
[128] J. Garcia, E. Gerjuoy, and J. Welker, Phys. Rev. **165**, 66 (1968).
[129] J. Hansen, Phys. Rev. A **8**, 822 (1973).
[130] V. Fock, Z. Phys. **98**, 145 (1935).
[131] C. Sheth, Phys. Rev. A **29**, 1151 (1984).
[132] E. J. McGuire, Phys. Rev. A **5**, 1043 (1972).